University of Reading

Characterization of peptides and their assemblies

Book or Report Section

Accepted Version

Hamley, I. W. ORCID: https://orcid.org/0000-0002-4549-0926 and Castelletto, V. (2020) Characterization of peptides and their assemblies. In: Guler, M. O. (ed.) Peptide-based Biomaterials. Royal Society of Chemistry, pp. 19-46. ISBN 9781788017299 doi: https://doi.org/10.1039/9781839161148-00019 Available at https://centaur.reading.ac.uk/94690/

It is advisable to refer to the publisher's version if you intend to cite from the work. See Guidance on citing.
Published version at: http://dx.doi.org/10.1039/9781839161148-00019
To link to this article DOI: http://dx.doi.org/10.1039/9781839161148-00019

Publisher: Royal Society of Chemistry

All outputs in CentAUR are protected by Intellectual Property Rights law, including copyright law. Copyright and IPR is retained by the creators or other copyright holders. Terms and conditions for use of this material are defined in the End User Agreement.

www.reading.ac.uk/centaur

CentAUR

Central Archive at the University of Reading

University of Reading

Reading's research outputs online

Characterization of Peptides and Their Assemblies

I. W. Hamley and V. Castelletto
Dept of Chemistry, University of Reading, Whiteknights, Reading RG6 6AD, U.K.

I.W.Hamley@reading.ac.uk.; V. Castelletto@reading.ac.uk Tel +44 118378 8453.

Running Head: Characterization of Peptide Assemblies

Keywords: Peptides, Conformation, Secondary Structure, Characterization Methods, Fluorescence Spectroscopy, Circular Dichroism, Linear Dichroism, FTIR spectroscopy, NMR, X-ray Diffraction, Light Scattering, Small-angle X-ray Scattering (SAXS), Small-Angle Neutron Scattering (SANS), Atomic Force Microscopy (AFM), Electron Microscopy, SEM, TEM, Analytical Ultrcentrifugation, Rheology

For "Peptide-Based Biomaterials", M.Guler (Ed), RSC Publishing

1. Introduction

Peptides are essential biomolecules and have a diversity of natural activities. Peptides are short chains of amino acids linked via amide bonds. There are twenty standard natural amino acids, with different side chains which confer particular bioactivity and biofunctionality. Amino acids can be grouped in different categories according to their chemical composition such as hydrophobic/ hydrophilic/ aliphatic/ aromatic/ or neutral/ positively/ negatively charged.[1] A diversity of non-natural amino acids has also been synthesized and incorporated into peptides to confer particular properties.

Intermolecular interactions between peptides allow for complex self-assembled nanostructures to develop. Particularly important are intra- and inter-molecular hydrogen bonds which control the type of secondary structure that may form. Additional interactions that influence peptide self-assembly include electrostatic interactions, hydrophobic interactions, aromatic interactions (π-π stacking) and van der Waals forces. The diverse properties of amino acids can be exploited in the design of peptides in order to control self-assembly to produce novel functional biomaterials.

There are two main classes of amphiphilic peptides; these are (i) designed purely peptidic systems with amphiphilic properties arising from sequences of hydrophobic and hydrophilic (charged) residues termed surfactant-like peptides (SLPs), and (ii) peptides modified by attachment of hydrophobic lipid chains these are termed peptide amphiphiles (PAs) or lipopeptides.[2]

This Chapter is focussed on methods to characterize the molecular conformation and self-assembly (leading to defined nanostructures) of peptides and peptide amphiphiles. This Chapter is organized as follows. The first section details methods to determine the critical aggregation concentration through fluorescence probe methods (Section 2). Then spectroscopic methods to characterize peptide secondary structure are considered including circular and linear dichroism (CD, LD; Section 3), Fourier transform infrared spectroscopy (FTIR), Raman spectroscopy (Section 4) and NMR spectroscopy (Section 5). The analysis of the structure of amphiphilic peptide assemblies using X-ray diffraction (XRD) is the subject of Section 6. We then turn to method to investigate fibrillization and the morphology of amphiphilic peptide self-

assemblies. Section 7 is concerned with light scattering, Section 8 with small-angle scattering methods and Section 9 with microscopic imaging technique, i.e. scanning probe and electron microscopies. Section 10 describes analytical ultracentrifugation (AUC). Section 11 discusses methods to characterise peptide gels such as rheology. The Chapter concludes with some brief summarizing remarks. This Chapter is not a review of the literature, but is intended as a guide to methodologies. As such we have mainly used data from our own publications for convenience, although of course papers from other groups will contain other excellent examples. This chapter is a modified and extended version of our recent contribution on the same theme.[3]

2. Fluorescence Methods – Labelling and Fluorescence Probe Assays

Fluorescence probe methods are widely used in the biosciences and as such have been utilized to investigate aspects of peptide aggregation in a number of ways. In this section, we discuss the use of fluorescence probe assays to determine the critical aggregation concentration (cac), analogous to the critical micelle concentration (cmc) of surfactants. In addition, we discuss dye staining methods such as the use of Congo red staining to detect amyloid. Molecular structures of fluorescent probe/dye molecules mentioned are shown in Figure 1.

Peptide amphiphiles can undergo aggregation into nanostructures above a critical aggregation concentration (*cac*) which is a more general term than critical micelle concentration (*cmc*) as observed for surfactants since it allows for aggregation into non-micellar structures. The *cac* may be detected via fluorescence methods. Pyrene is a fluorescent probe molecule which is used to locate the *cac* for conventional

amphiphiles, as its fluorescence is sensitive to the local hydrophobic environment.[4, 5] It has also successfully been used to determine the *cac* for several PA systems.[6-17] Pyrene fluorescence measurements of *cac* usually involve determination of the ratio of third and first vibronic band intensities, I_{373}/I_{383} or I_1/I_3, although sometimes I_1 itself shows discontinuities at the same concentration.[13, 18] For conventional amphiphiles, I_1/I_3 decreases at the critical micelle concentration, from a typical value around 1.7-1.8 to a lower value 1.0-1.2 [see, for example ref.[19, 20]], although this is not always observed for lipopeptides, in particular if they contain an aromatic residue which contributes to UV absorbance. Pyrene derivatives such as 1-pyrene carboxylic acid offer lower toxicity than pyrene itself and have been successfully used in amyloid peptide cac determination.[21] We have recently used the fluorescent probe ANS (8-anilino-1-naphthalenesulfonic acid, Fig.1) to locate critical aggregation concentrations of a range of lipopeptides and SLPs.[22-24] Like pyrene, ANS fluorescence is also sensitive to the local hydrophobic environment.[22, 23, 25-27] It shows good fluorescence sensitivity and is less toxic than pyrene. A further possibility for peptides containing tryptophan is to use the intrinsic tryptophan fluorescence to locate the *cac*, this has been shown to successfully detect the same *cac* value as pyrene fluorescence.[28]

In contrast to use of pyrene or ANS, the fluorescence of Thioflavin T (ThT) is dependent on the formation of amyloid-like structures (β-sheet fibrils) [29, 30] and has been used for amyloid fibril-forming peptides. Excitation of ThT at 450 nm produces fluorescence at 482 nm.[29, 31] ThT can be used to determine the *cac* of lipopeptide PAs, the value obtained being similar to that obtained from pyrene fluorescence techniques in the case that amyloid fibril formation occurs at the same concentration as

hydrophobic collapse.[8, 12, 13] This is not always the case. Figure 2 compares assays to obtain *cac* values from ANS fluorescence with those using ThT for two amyloid peptides based on the KLVFF core motif[32, 33] of the Amyloid β (Aβ) peptide.[23] For NH_2-KLVFF-$CONH_2$, the *cac* measured by both techniques is the same (within uncertainty) showing that fibril formation and hydrophobic collapse occur at the same concentration for this sample. However, for the blocked analogue peptide NH_2-K(Boc)LVFF-$CONH_2$, the *cac* determined from the concentration dependence of ANS fluorescence is significantly lower than that from the ThT probe assay. This suggests that hydrophobic collapse occurs at a lower concentration than that at which fibril formation occurs.[23] In the intermediate concentration range, presumably small oligomeric structures with hydrophobic interiors are present. ThT fluorescence has also been widely used probe the kinetics of amyloid aggregation processes.[33, 34] This phenomonen has also been observed for $A_{10}H_6$[35] and

Other fluorescent dyes such as Nile red (Fig.1) have been used to determine the *cac* of amyloid-forming peptides,[36, 37] but have not yet been widely employed in studies of PA systems. The fluorescent probe DPH [1,6-diphenyl-1,3,5-hexatriene] (Fig.1) has also been used to locate the cac of lipopeptides.[38]

Staining with fluorescent dyes is used in confocal microscopy and has been applied to image micron-scale self-assemblies. For example, the lipopeptide “Matrixyl” C16-KTTKS forms highly extended nanotape structures which were imaged by confocal microscopy using Rhodamine B staining.[39] Congo red staining provides a method

that, by definition, identifies amyloid.[34] Under polarized light, amyloid samples exhibit green birefringence when stained with Congo red. Figure 3 shows an example of a polarized optical microscopy (POM) image of an β-sheet forming lipopeptide stained with Congo red, showing the green birefringence texture.[40]

Förster resonance energy transfer (FRET) has been used to investigate the binding of dye to amyloid fibrils.[41]

3. Circular and Linear Dichroism

Cicular dichroim (CD) is a technique to probe the secondary structure of proteins and peptides. The method relies to the differential absorption of right- and left- circularly polarized light. The usual method is based on "fingerprinting" of spectral features in the 190-250 nm far UV region.[42-44] Data in the near UV region can provide information on the conformation of peptides containing aromatic residues with absorption features in the 250-310 nm range. In the far UV region, characteristic minima are observed in the absorption spectra at (approximately) 208 and 222 nm (α-helix) or 216-220 nm (β-sheet) as shown in the spectra in Fig.4a. On the other hand, a broad weak minimum in the range 195-200 nm is characteristic of disordered, sometimes known as random coil conformation (Fig.4b). This can be contrasted with the spectra for The polyproline II (PPII) conformation which is characterized by a deep minimum in the CD spectrum at around 190-205 nm, along with a broad positive maximum at around 215-225 nm (Fig.4b).[45-48] Examples showing the comparison between CD spectra for PPII and disordered conformation can be found in the literature.[47, 49] The CD spectra for the main secondary structures structures are

characterized by typical values of the molar (or alternatively mean residue) ellipticity [43, 50], as well as the position of the maxima/minima. In fact, CD spectra should be normalized in this way (Eq.1) for this reason, and also to facilitate comparison between samples at different concentration or measurements in different path length cells. The molar ellipticity is given by

$$[\theta] = \frac{\theta}{10cl} \quad (1)$$

Here [θ] is the molar ellipticity (in units deg cm^2 dmol^{-1}), θ is the measured CD signal amplitude in millidegrees (mdeg), c is the molar concentration and l is the path-length of the cell in cm. The magnitude of the mean residue ellipticity (MRE, molar ellipticity divided by number of residues) can be used to determine the α-helical content of coil peptides,[51] and comparison of the ratio of the molar ellipticity at 222 and 208 nm gives information on the coiled coil content.[51] A recent example of the use of this analysis for coiled-coil forming peptides based on the gut hormone PYY explores the effect of lipidation and PEGylation on the conformation and self-assembly.[52]

CD spectra for proteins are usually analysed using algorithms based on databases compiled for proteins for which the x-ray crystal structure is known.[43] This permits an accurate determination of secondary structure content which can be used to "calibrate" CD spectra. A range of software is available based on various databases, see for example refs.[53-56] Most consider only larger proteins although there are limited reference data sets (and curve fitting programs) for shorter peptides.[57] This type of analysis is of little use for small peptids or lipopeptides for which individual residues

(especially aromatic residues) and specific conformations (e.g. turns) can dominate the CD spectrum.

Linear dichroism refers to the differential absorbance of plane polarized UV radiation, and it gives information on the alignment of extended objects resulting from peptide self-assembly. Since amyloid fibrils and nanotapes are highly anisotropic, they can align under flow or other fields and this can be probed using LD which in particular provides information on the orientation of the peptide backbone and of chromophores such as aromatic residues.[42, 44, 50, 58]

4. FTIR and Raman Spectroscopy

FTIR is sensitive to the vibrational modes of bonds within peptides. Specific regions of the spectrum are the focus of particular analysis. Specifically, the amide I region in the range 1600-1700 cm^{-1} is sensitive to the modes of CO, CN and NH groups[59] which are influenced by H-bonding. A prime is added to the name of the region of the spectrum, for example to give the term amide I′ for spectra measured in D_2O. All band positions mentioned above are slightly downshifted if measurements are performed in D_2O.[60] In fact, measurements in D_2O are beneficial since water absorption features around 1650 cm^{-1} can be avoided. Our group always perform measurements in D_2O solutions. In our experience, peptide concentration must be 0.5 wt% or more typically to obtain a reliable signal. It is also quite common to perform FTIR on dried samples in the form of films for transmission mode measurements or via ATR (attenuated total reflectance) measurements.

The amide I region gives information on secondary structure, via "fingerprinting" or peak fitting methods.[59, 61] These are prone to uncertainty associated with the overlap of features in the spectra [59, 61, 62] although clear features of secondary structures such as β-sheets can be resolved by performing measurements in transmission mode on a modern FTIR instrument, with sufficiently concentrated samples in D_2O in narrow path-length cells. A band typically in the 1620-1640 cm^{-1} range is associated with β-sheet structures.[59, 61-64] A band in the typical range 1648 – 1657 cm^{-1} is associated with α-helix structure whilst disordered peptides give a peak in the typical range 1642-1650 cm^{-1}. [59, 60, 62] The narrow intense band observed for some peptides at 1675-1695 cm^{-1} is usually ascribed to antiparallel β-sheet structure.[60] Caution is required since a peak in the amide I region of an FTIR spectrum at 1673 cm^{-1} is due to residual trifluoroacetic acid from the peptide synthesis bound to peptide cations (unless this is removed by ion exchange methods).[61, 64-67]

The amide II band around 1550 cm^{-1} mainly results from the N-H bending vibrations which are responsive to deuteration (the deuterium from D_2O exchanges positions with hydrogen from the N-H bond).[59] As a consequence the amide II' band is shifted by approximately 100 cm^{-1} to 1450 cm^{-1} in D_2O.[68]

Tables of specific side-group FTIR bands are available.[60, 69, 70] In addition, a peak near 1705 cm^{-1} may be assigned to carbonyl stretch, e.g. in acidic side residues or from the C terminus.[11, 60, 71, 72] Information on lipid chain CH_2 deformations in lipopeptides is provided by peaks in the 2800-3000 cm^{-1} range of the spectra.[22]

Isotope labelling of peptides enables specific features in the FTIR spectrum to be resolved as bands associated with deformation modes of labelled residues will be shifted .[73-76]. Typically, isotopic substitution using ^{13}C-labelled peptide splits amide I bands for β-sheets into higher and lower frequency peaks. The magnitude of the ^{12}C wavelength shift depends on the extent of perturbation of the ^{12}C carbonyl coupling induced by ^{13}C substitution and strongly coupled β-sheets are generally sensitive to such isotopic substitution.[74] This can be used to infer information on the registry of β-strands.[73, 74]

FTIR can be extended to study linear dichroism (polarized FTIR) on aligned samples with isotope labelling[75, 77] and to vibrational circular dichroism.[63] Vibrational circular dichroism (VCD) is analogous to (UV) electronic CD, but evidently extended to the IR mode, sensitive to bond vibrations.[78, 79] The analogous technique using Raman scattering is Raman Optical Activity (ROA).[78] Polarized Raman spectroscopy can provide information on the orientation of specific features such as aromatic residues.[58]

Recently, 2D IR methods have attracted great interest as it is possible to correlate vibrational modes, providing information on mode coupling. When combined with isotope editing of peptides, 2D IR can provide detailed information on β-sheet conformation and the pathway of amyloid formation in amyloid peptides such as human islet amyloid polypeptide, hIAPP.[80, 81] In another example, the method was used to investigate the PPII conformation of di-alanine.[82]

Raman spectra provide similar information on peptide secondary structure (the transition rules are generally satisfied for peptide deformation modes for both Raman and FTIR spectroscopy) and side chain deformation modes to FTIR,[8] although this technique is less commonly available in the laboratory. As it is a scattering-based method, Raman spectroscopy also typically requires a higher sample concentration than FTIR to get a useful spectrum. However, measurement of Raman spectra can be recorded in H_2O in contrast to FTIR where the water absorption band prevents measurements in the vital amide I region. Raman microscopy enables the chemical mapping of peptide samples scanning across the sample at micron resolution and measuring Raman spectra. In one example, the cell-penetrating peptide penetratin secondary structure within live cells was detected by Raman microscopy, using a peptide labelled with ^{13}C-Phe (and adjacent ^{15}NH amide).[83]

5. NMR Spectroscopy

This section does not consider the routine use of NMR to analyse syntheized protein structures, but rather focussed on specialised NMR techniques to probe peptide aggregates.

Solution NMR can be used to provide high resolution peptide structures, such as those of helical peptides via 2D correlation methods such as TOCSY, COSY or NOESY. One example of interest to our group is the NMR study of the conformation of the human gut peptide hormone PYY_{3-36}, which showed which residues are in the helical

domain.[84] This is relevant to our studies on the aggregation and conformation of analoguous lipidated or PEGylated PYY_{3-36} peptides, with different positions of lipidation and PEGylation with respect to the helical domain.[17, 52]

The aggregation state of many peptides has been probed using solution ^{1}H NMR. For example, the degree of ionization of the C terminus of a model amyloid peptide has been studied as a function of concentration.[49] Likewise, ^{1}H NMR solubility measurements have been used to obtain solubility phase diagrams and related diffusion measurements have enabled the critical micelle concentration of a lipopeptide to be obtained.[85] Specific chemical information, for information on metal ion binding to peptides can also be obtained from solution ^{1}H NMR.[86] In a recent study ^{1}H NMR has been used to probe aggregation in proline-rich surfactant-like peptides P_6K and P_6E, which form vesicle-like structures at 80 ºC.[87] On heating to this temperature from 25 ºC, NMR visible species were reduced to ca. 50% using an internal standard for integration. This fact proves the formation of large, NMR-silent aggregates (which were imaged by cryo-SEM and sized using DLS). In addition, ^{1}H NMR spectra revealed that the multiplicity pattern of the signals corresponding to the diasterotopic protons at position 3 in the proline ring is heavily modified (Fig.5), indicating important conformational changes and changes of $^{1}H–^{15}N$ long-range correlations, carried out for both peptides ^{15}N-enriched sample at the fifth proline proline, also revealed important changes in the complex multiplicity pattern of the signals corresponding to the proline ring.[87]

Solid state NMR (ssNMR) has provided much detail on amyloid fibril structure. A number of high resolution experiments employing magic angle spinning may be

performed using isotopically labelled ^{13}C or ^{15}N peptides.[88-91] For example, the peptide KLVFFAE [Aβ(16-22)] has been found to adopt an antiparallel β-sheet arrangement through ss NMR,[92] and isotope-edited FTIR on labelled peptides (combined with ssNMR) [73, 74] and computer simulation.[93] Information on peptide β-strand alignment within nanotubes (based on line-shape analysis) was obtained from ssNMR spsctra obtained from aligned films of labelled variants of the surfactant-like peptide A_6K including measurement of ^{2}H and ^{15}N spectra for peptides labelled with these isotopes at specific alanine residues provided.[76] Homo-nuclear and hetero-nuclear 2D and 3D NMR spectroscopy enable information on interatomic distances and torsion angles to be obtained for isotopically labelled peptides in the dried state.[94, 95]

Hydrogen/deuterium exchange techniques have also been employed to probe structural changes during amyloid aggregation.[94] Information on structural rearrangements of subsegments of a protein or peptide during folding, unfolding or fibrillisation cab be obtained from exchange rate measurements. This method has also been used to provide a 3D structure for the Amyloid β peptide Aβ42.[96]

6. X-ray Diffraction

Single crystal x-ray diffraction can be used to obtain the crystal structure of peptides, although there are relatively few reports on this for aggregating peptides and lipopeptides due to the difficulty in growing a crystal from a sample in which self-assembly occurs (in preference to crystal formation). In particular, with a very few

exceptions, amyloid peptides and lipopeptides do not crystallize, prohibiting single crystal X-ray diffraction. This is because fibrillar assemblies are by their nature non-crystalline, one or two-dimensional arrays with a low degree of molecular ordering. With careful preparation, it is possible to obtain single crystal XRD patterns from small amyloid peptide fragments.[97-100]

Fibre diffraction is an alternative to single crystal XRD which is particularly suited to analyse the structure of peptides which form fibrilla assemblies, including amyloid peptides, coiled coil peptides, lipopeptide fibrils and peptide nanotubes.
Amyloid peptide fibrils comprise bundles of β-sheets with backbones orthogonal to the fibre axis, in the so-called "cross-β" structure [101-105]. Fig.6 shows a high quality fibre XRD pattern from the PA C_{16}-GGGRGDS,[11] which contains the RGDS cell adhesion motif (key short peptide motifs such as RDGS have been discussed in a recent review[106]). This is obtained from a stalk dried from a concentrated solution at the end of a wax-coated capillary.[107] The signature in an X-ray scattering pattern of the cross-β structure is a 4.7 Å meridional reflection corresponding to the spacing between peptide backbones and at least one equatorial reflection with a d-spacing 8-14 Å which corresponds to the stacking of β sheets. In the case of the pattern in Fig.6 there are additional equatorial reflections. In general, multiple such reflections come from molecular and β-sheet periodicities (for example the long spacing 52.3 Å is assigned to a bilayer periodicity,[11]). Unit cell parameters can be obtained by indexing cross-β fibre XRD patterns and this can be performed using software such as CLEARER.[108] Fibre XRD is performed on dried films. In one study, the effect of hydration has been examined. coworkers have examined whether the cross-β structure is retained in flow-aligned solution.[109] The wide angle X-ray scattering (WAXS)

patterns for a peptide and a protein sample subjected to flow-alignment showed the same pattern as for the corresponding dried samples, indicating that the cross-β structure is present in solution and is not an artefact caused by dehydration. Fibrils are other classes of peptides such as those adopting coiled-coil conformations and these have distinct XRD patterns.[110, 111]

As mentioned above, fibre XRD is performed on dried samples, in the form of films or "stalks", the latter being dried threads of solution. Other methods of alignment include the use of stretch frames or cryo-loops, the latter producing a dried flat film or "mat".[112]

7. Dynamic and Static Light Scattering

In dynamic light scattering (DLS, sometimes known as photon correlation spectroscopy), analysis of the intensity autocorrelation function of scattered light from a particle undergoing translational or rotational diffusion enables determination of a diffusion coefficient, and hence via the Stokes-Einstein equation, the effective hydrodynamic radius.

Static light scattering (SLS) can be used to obtain the molecular weight of peptide aggregates and also to provide an indication on particle shape, via measurements of the angular dependence of the scattered intensity. The angular dependence of the scattered light from amyloid fibrils in an SLS experiment can provide information on the conformation of amyloid fibrils, for example whether stiff, flexible or branched. Murphy and coworkers have applied linear and branched wormlike chain models to

describe static light scattering data from Aβ alone and also from mixtures of Aβ with Aβ fragments [including Aβ(16-20)] [113]. They also reported a branched wormlike chain form factor [113, 114]. We have used this method to fit SLS data from Aβ fragment peptide KLVFF [32].

Dynamic light scattering has been used to monitor the formation of amyloid protofilaments and fibrils [115-118] in the sense that it can distinguish between monomers, oligomers and larger structures. However, DLS provides the translational diffusion coefficient based on the assumption of spherical particles (in the case of the usual Stokes-Einstein) equation.[119, 120] The analysis is more complex for anisotropic particles since the decay of the correlation function depends on both the rotational and translational diffusion coefficients.[121] These can be decoupled in depolarized dynamic light scattering (DDLS).[121]

8. Small-Angle Scattering

Small-Angle X-ray Scattering (SAXS) and Small-Angle Neutron Scattering (SANS) are powerful complementary techniques to probe the nanostructure of self-assembled objects such as peptide assemblies. SAXS can be performed in the laboratory or at a central synchrotron facility, whereas SANS is performed using either a spallation or nuclear reactor as the source of neutrons. In either technique, the variation of the scattered intensity with $q = 4\pi\sin\theta/\lambda$ (2θ is the scattering angle and λ is the wavelength) provides information on the interaction between self-assembled objects via the structure factor, and also on the shape and scattering density profile (from the form factor). Since X-rays are scattered by electrons, a SAXS form factor depends on the electron density profile, whereas SANS provides information on the scattering

length density profile (this depends on the nuclear scattering factors). In dilute solution, only form factor scattering is obtained and this is used to obtain the dimensions of the peptide assembly. SAXS offers the potential for fast time-resolved measurements and higher throughput measurements. SANS enables contrast variation measurements using H_2O/D_2O mixtures,[122] and longer measurements without the risk of beam damage of samples (leading to ionisation and molecular dis-assembly) which can occur with synchrotron SAXS. In our experience on various SAXS and SANS beamlines, both techniques can be employed for solutions down to around 0.1 wt% (1 mg/ml) although we usually study samples with above 5 mg/ml of peptide.

The SAXS form factor from unaggregated peptide can readily be distinguished from that of peptide assemblies, as shown through the examples presented in Fig.7. Fig.7b shows the shape of a monomer form factor, which has been fitted with a so-called Gaussian coil model to represent the unordered conformation. It has a characteristic flat shape at low *q*, curving over at high *q*. The shape of this form factor can be contrasted from those of the assembled structures shown in Fig.7.

SAXS data from lipopeptide/peptide micelles has been fitted using a core-shell (two electron density level) sphere form factor, [17, 18, 52, 85, 123-125] an example being shown in Fig.7d. This figure also shows the influence of the structure factor (solid red line model fit) which leads to a broad peak at low *q*. For the spherical micelle case, the structure factor may be the simple hard-sphere structure factor model as in the fit in Fig.7d (the corresponding fit parameters are listed in Table 1).

For amyloid fibrils, a uniform[126] or core-shell[127] cylinder form factor can be used to fit SAXS or SANS data. A representative fit is shown in Fig.7f. A core-shell model is generally required since there is usually a contrast difference between the core of the peptide fibril and the exterior. This is particularly evident for instance in the case of PEG-peptides with a PEG corona.[127, 128]

For nanotapes formed in particular (but not exclusively) by lipopeptides we have found that a form factor developed for lipid bilayers can successfully be employed. This so-called Gaussian bilayer form factor comprises three Gaussian functions, one of which represents the electron density (in the case of SAXS) of the lipid-chain rich core (negative amplitude), the other two being (positive amplitude) Gaussians representing the electron density of the charged head-groups (Fig.7g). The corresponding parameters are shown in Fig.8 and the form factor equations and definitions can be found in the original paper where this form factor was reported,[129] or our recent papers utilising this form factor.[9, 11, 130]

We have extensively used the software SASfit [131] to fit form factor data from amphiphilic peptide assemblies. The software includes many different form factors including those described above and many others, and it also has a powerful least-squares fitting algorithm. Other data to fit SAS data is available including SASView,[132] and GENFIT[133] or FISH (SANS specific).[134] In addition, software is available to calculate SAS profiles from pdb files (which can be constructed or generated from simulations of peptide assemblies) including Crysol[135]/Cryson (x-ray and neutron versions) available within the ATSAS SAS data analysis and modelling package[136] and FoXS.[137, 138] and others.[139]

The remarkable assembly of amphiphilic peptides into nanotubes has also been observed, and data have been fitted with corresponding form factors (e.g. Fig.6j).[130, 140, 141] If the nanotube radius $R >> t$, where t is the tube wall thickness (e.g. of a bilayer) then the Gaussian bilayer form factor used above can be used to fit the high q part of the small-angle scattering data.[142]

Further information on peptide samples that either exhibit the formation of lyotropic liquid crystal phases (e.g. nematic, hexagonal-packed cylinder or lamellar) or which align under shear flow, can be obtained through small-angle scattering. At most synchrotron SAXS beamlines (and on many lab instruments) and SANS instruments the data is measured on a 2-dimensional area detector and it is straightforward to check the original SAXS or SANS pattern (before reduction to 1-dimensional intensity profiles) to check for sample alignment which is manifested in anisotropy in the SAS pattern. In some cases, spontaneous alignment of the sample is observed. We have noted this phenomenon with several peptide and lipopeptide samples (forming aligning fibril or nanotube structures) when flowing them through a capillary at SAXS and BioSAXS beamlines (see for example, ref.[142]). However, orientation is best studied under precisely defined flow conditions such as steady shear (with a Couette cell for example, Fig.9) or with simultaneous rheology and SAXS or SANS (rheoSAXS or rheoSANS). Representative SANS data obtained for a peptide nanotube solution in a commercial rheometer are shown in Fig.10.[141] The SANS pattern (here the data corresponding to the radial configuration in Fig.9 is shown)

develops anisotropy under steady shear, although this is lost upon cessation of shear (i.e. this sample only aligns under flow).

9. Electron Microscopy and Scanning Probe Microscopy

These methods provide direct imaging of peptide fibrils. Atomic force microscopy (AFM) which is a scanning probe microscopy provides images at the surface. To date,the method has mainly been used to image fibrils from solutions dried onto planar solid substrates such as mica. The use of AFM to study amyloid fibrils has been reviewed.[143] Recent developments include sophisticated analysis software which can be used to quantify the properties of amyloid fibrils including conformation, stiffness, orientation etc.[144-146] Measurement of fiber mechanical properties using peak force microscopy with an AFM instrument has now yielded values of the elastic modulus for many amyloid fibril systems.[143, 147] Fig.11 shows a nice example of AFM height images taken during the aggregation process of an Aβ peptide-based fragment based peptide which forms twisted tapes, then ribbons and then finally, after low temperature incubation, nanotubes.[148]

There are two main types of electron microscopy. Conventional transmission electron microscopy (TEM) is performed on dried films on carbon grids (these are usually stained with heavy-metal containing compounds to enhance contrast). Scanning electron microscopy (SEM) is used to image surfaces of pieces of a sample, most typically prepared by drying, although frozen or partially hydrated specimens can be imaged by cryo-SEM or environmental SEM (ESEM) respectively. Cryogenic techniques in cryogenic-TEM involve cooling the sample to -187 ^{o}C in liquid ethane

to vitrify the aqueous phase. This technique avoids artefacts caused by slow drying, exemplified by images for Aβ fragment peptide KLVFF – cryo-TEM clearly shows extended fibril structures which were not observed in conventional TEM.[32] In our experience, cryo-TEM is the best imaging technique for amphiphilic peptide nanostructures. Reviews of the topic are available.[149-151] Fig.12 shows representative cryo-TEM images from different classes of peptide nanostructures.

In our opinion, SEM images should be interpreted with a degree of scepticism since a "fibrillar network" morphology is observed for many peptide structures on the micron lengthscale which is not related to the individual nanostructure elements such as fibrils with 1-10 nm diameters, which can be resolved using (cryo)TEM or AFM. Fig.13 shows a representative cryo-SEM image of nanotapes formed by self-assembly of a β-sheet –forming peptide.

In some cases, amphiphilic peptide assemblies such as fibrils or nanotapes are large enough to be imaged by optical microscopy – see for example ref. [39]

10. Analytical Ultracentrifugation

Analytical ultracentrifugation involves centrifuging a peptide solution at very high rotation speeds (angular accelerations ~10,000s of g) in order to determine the distribution of species, monomers and oligomers, present in a sample.[152, 153] This can be used for example to analyse the formation of coiled coils[52, 154] or small amyloid oligomers.[155-157] The sedimentation coefficient can be obtained and, with an estimate for the frictional ratio which accounts for the deviation from spherical shape of the particles, this can be used to obtain molar masses for the species present. AUC can be

used for species with molar masses in the range from 100 Da up to megadaltons. The data is processed using software such as SEDFIT.[158]

11. Gel Characterization Methods

A large number peptides will form hydrogels under appropriate conditions (sufficiently high concentration, adjustment of pH etc), especially under conditions where fibril formation is favoured. These hydrogels are useful in the development of peptide-based biomaterials such as scaffolds for cell growth and differentiation or as slow release systems.[159] Peptide-based molecules are also capable to act as organogelators with applications in oil/pollutant recovery and catalysis, among others.[160, 161]

Rheology refers to the study of the flow properties of materials. It is a powerful technique to investigate the dynamic mechanical behaviour of peptide materials, in particular to measure the ridigity of peptide gels. The most common type of experiment to characterize peptide gels is to measure the dynamic shear moduli in controlled stress or controlled strain shear rheometer. The gel is typically placed in a cone-and-plate or plate-plate geometry and subjected to oscillatory shear or strain. The frequency-dependent measurements provide the dynamic elastic shear modulus, G', and the dynamic loss shear modulus, G''. The measurements are performed in the linear viscoelastic regime, which is identified by first performing a stress or strain sweep to identify a stress or strain value within the range where the moduli (at a fixed frequency) do not depend on the stress or strain (typically the highest value in the range, to minimize noise on the measured data). Figure 14 shows typical frequency-

dependent modulus data for two samples of peptide amphiphiles. The PA C_{16}-GGGRGD forms a stiff hydrogel which is characterized by $G' > G''$ with both moduli largely independent of frequency. In contrast, the PA C_{16}-GGGRGDS does not form a hydrogel, the strong frequency dependence of the moduli and the fact that by $G'' > G'$ are both properties that are characteristic of a liquid.[122, 162]

Gels are sample-spanning networks. In the case of peptides, gels are often formed from entangled fibrils. The structure is best determined by *in situ* small-angle scattering measurements. Imaging of gel morphology is typically carried out using SEM or cryo-SEM (remembering the note of caution mentioned above about interpretation of SEM images).[163] Samples for TEM, cryo-TEM or AFM must be diluted in order to cover the grid or surface, and of course this disrupts the gel structure.

Summary

In summary, a variety of methods are available to investigate the self-assembly of amphiphilic peptides. Often it is first of interest to determine the critical aggregation concentration, if present, from concentration-dependent fluorescent probe intensity measurements. Then spectroscopic methods can be used to probe molecular conformation (NMR), chiral ordering (CD), and hydrogen bonding (FTIR). Molecular packing can be studied using fibre XRD which is appropriate to the typical extended fibrillar and tape structures formed by β-sheet amphiphilic peptide assemblies. Small-angle scattering provides in situ techniques to determine the

morphology and dimensions and scattering density profile of self-assembled structures. We generally complement SAXS or SANS data with cryo-TEM images or AFM images to provide a comprehensive characterization of nanostructure. Gels are often fibrillary structures, which can be imaged by SEM and their mechanical properties are measured via shear rheology.

Acknowledgements. This work was supported by EPSRC Platform Grant EP/L020599/1. We thank current and previous group members for their contributions to our research. We are also grateful to our collaborators for their vital contributions to several aspects of our ongoing research, especially in the fields of AFM imaging (Prof Raffaele Mezzenga and Dr Jozef Adamcik, ETH Zürich) and cryo-TEM imaging (Prof Janne Ruokolainen and his team at Aalto University, Finland).

References

1. T. E. Creighton, *Proteins. Structures and Molecular Properties*, W.H.Freeman, New York, 1993.
2. I. W. Hamley *Soft Matter*, 2011, **7**, 4122-4138.
3. V. Castelletto and I. W. Hamley, in *Peptide Self-Assembly: Methods and Protocols*, eds. B. L. Nilsson and T. M. Doran, Humana Press Inc, Totowa, 2018, vol. 1777, pp. 3-21.
4. K. Kalyanasundaram and J. K. Thomas, *J. Am. Chem. Soc.*, 1977, **99**, 2039-2044.
5. F. M. Winnik, *Chem. Rev.*, 1993, **93**, 587-614.
6. M. O. Guler, R. C. Claussen and S. I. Stupp, *J. Mater. Chem.*, 2005, **15**, 4507-4512.
7. R. Sabate and J. Estelrich, *J. Phys. Chem. B*, 2005, **109**, 11027-11032.
8. V. Castelletto, G. Cheng, B. W. Greenland and I. W. Hamley, *Langmuir*, 2011, **27**, 2980-2988.
9. V. Castelletto, G. Cheng, C. Stain, C. J. Connon and I. W. Hamley, *Langmuir*, 2012, **28**, 11599-11608.
10. R. R. Jones, V. Castelletto, C. J. Connon and I. W. Hamley *Molec. Pharm.*, 2013, **10**, 1063-1069.

11. V. Castelletto, R. J. Gouveia, C. J. Connon and I. W. Hamley *Faraday Disc.*, 2013, **166**, 381-397.
12. I. W. Hamley, A. Dehsorkhi and V. Castelletto, *Langmuir*, 2013, **29**, 5050-5059.
13. V. Castelletto, R. J. Gouveia, C. J. Connon, I. W. Hamley, J. Seitsonen, A. Nykänen and J. Ruokolainen, *Biomater. Sci.*, 2014, **2**, 362-369.
14. M. Fowler, B. Siddique and J. Duhamel, *Langmuir*, 2013, **29**, 4451-4459.
15. I. W. Hamley, J. Hutchinson, S. Kirkham, V. Castelletto, A. Kaur, M. Reza and J. Ruokolainen, *Langmuir*, 2016, **32**, 10387-10393.
16. E. R. Silva, E. Listik, S. W. Han, W. A. Alves, B. M. Soares, M. Reza, J. Ruokolainen and I. W. Hamley, *Biophys. Chem.*, 2018, **233**, 1-12.
17. J. A. Hutchinson, S. Burholt, I. W. Hamley, A.-K. Lundback, S. Uddin, A. G. dos Santos, M. Reza, J. Seitsonen and J. Ruokolainen, *Bioconjugate Chem.*, 2018, **29**, 2296-2308.
18. I. W. Hamley, S. Kirkham, A. Dehsorkhi, V. Castelletto, M. Reza and J. Ruokolainen, *Chem. Comm.*, 2014, **50**, 15948-15951.
19. M. Wilhelm, C.-L. Zhao, Y. Wang, R. Xu, M. A. Winnik, J.-L. Mura, G. Riess and M. D. Croucher, *Macromolecules*, 1991, **24**, 1033-1040.
20. M. Johnsson, P. Hansson and K. Edwards, *J. Phys. Chem. B*, 2001, **105**, 8420-8430.
21. C. C. Decandio, E. R. Silva, I. W. Hamley, V. Castelletto, M. S. Liberato, V. X. Oliveira, C. L. P. Oliveira and W. A. Alves, *Langmuir*, 2015, **31**, 4513-4523.
22. V. Castelletto, S. Kirkham, I. W. Hamley, R. Kowalczyk, M. Rabe, M. Reza and J. Ruokolainen, *Biomacromolecules*, 2016, **17**, 631-640.
23. V. Castelletto, P. Ryumin, R. Cramer, I. W. Hamley, M. Taylor, D. Allsop, M. Reza, J. Ruokolainen, T. Arnold, D. Hermida-Merino, C. I. Garcia, M. C. Leal and E. Castaño, *Sci. Rep.*, 2017, **7**, 43637.
24. I. W. Hamley, V. Castelletto, A. Dehsorkhi, J. Torras, C. Aleman, I. Portnaya and D. Danino, *J. Phys. Chem. B*, 2018, **122**, 1826-1835.
25. M. Lindgren, K. Sorgjerd and P. Hammarstrom, *Biophys. J.*, 2005, **88**, 4200-4212.
26. O. K. Gasymov and B. J. Glasgow, *Biochim. Biophys. Acta-Proteins and Proteomics*, 2007, **1774**, 403-411.
27. A. Hawe, M. Sutter and W. Jiskoot, *Pharm. Res.*, 2008, **25**, 1487-1499.
28. B. M. Soares, A. M. Aguilar, E. R. Silva, M. D. Coutinho-Neto, I. W. Hamley, M. Reza, J. Ruokolainen and W. A. Alves, *Phys. Chem. Chem. Phys.*, 2017, **19**, 1181-1189.
29. H. LeVine, *Protein Sci.*, 1993, **2**, 404-410.
30. H. LeVine, in *Methods in Enzymology*, ed. R. Wetzel, Academic Press, San Diego, 1999, vol. 309, pp. 274-284.
31. S. J. Wood, B. Maleef, T. Hart and R. Wetzel, *J. Molec. Biol.*, 1996, **256**, 870-877.
32. M. J. Krysmann, V. Castelletto, A. Kelarakis, I. W. Hamley , R. A. Hule and D. J. Pochan, *Biochemistry*, 2008, **47**, 4597-4605.
33. I. W. Hamley *Chem. Rev.*, 2012, **112**, 5147-5192.
34. I. W. Hamley *Angew. Chem., Int. Ed. Engl.* 2007, **46**, 8128-8147.
35. I. W. Hamley, S. Kirkham, A. Dehsorkhi, V. Castelletto, J. Adamcik, R. Mezzenga, J. Ruokolainen, C. Mazzuca, E. Gatto, M. Venanzi, E. Placidi, P. Bilalis and H. Iatrou, *Biomacromolecules*, 2014, **15**, 3412-3420.

36. M. K. Santra, A. Banerjee, S. S. Krishnakumar, O. Rahaman and D. Panda, *Eur. J. Biochem.*, 2004, **271**, 1789-1797.
37. S. Jha, J. M. Snell, S. R. Sheftic, S. M. Patil, S. B. Daniels, F. W. Kolling and A. T. Alexandrescu, *Biochemistry*, 2014, **53**, 300-310.
38. M. van den Heuvel, H. Baptist, P. Venema, E. van der Linden, D. Löwik and J. C. M. van Hest, *Soft Matter*, 2011, **7**, 9737-9743.
39. V. Castelletto, I. W. Hamley, J. Perez, L. Abezgauz and D. Danino, *Chem. Comm.*, 2010, **46**, 9185-9187.
40. V. Castelletto, A. Kaur, R. M. Kowalczyk, I. W. Hamley, M. Reza and J. Ruokolainen, *Biomacromolecules*, 2017, **18**, 2013-2023.
41. M. Girych, G. Gorbenko, V. Trusova, E. Adachi, C. Mizuguchi, K. Nagao, H. Kawashima, K. Akaji, S. Lund-Katz, M. C. Phillips and H. Saito, *J. Struct. Biol.*, 2014, **185**, 116-124.
42. A. Rodger and B. Nordén, *Circular Dichroism and Linear Dichroism*, Oxford University Press, Oxford, 1997.
43. S. M. Kelly, T. J. Jess and N. C. Price, *Biochim. Biophys. Acta*, 2005, **1751**, 119-139.
44. B. Nordén, A. Rodger and T. R. Dafforn, *Linear Dichroism and Circular Dichroism: A Textbook on Polarized-Light Spectroscopy* RSC, Cambridge, 2010.
45. R. W. Woody, *Meth. Enzymol.*, 1995, **246**, 34-71.
46. Z. S. Shi, R. W. Woody and N. R. Kallenbach, in *Unfolded Proteins*, ed. G. D. Rose, Academic Press Inc, San Diego, 2002, vol. 62, pp. 163-240.
47. S. E. Paramonov, H.-W. Jun and J. D. Hartgerink, *J. Am. Chem. Soc.*, 2006, **128**, 7291-7298.
48. R. W. Woody, *J. Am. Chem. Soc.*, 2009, **131**, 8234-8245.
49. V. Castelletto, I. W. Hamley , C. Cenker, U. Olsson, J. Adamcik, R. Mezzenga, J. F. Miravet, B. Escuder and F. Rodriguez-Llansola, *J. Phys. Chem. B*, 2011, **115**, 2107-2116.
50. B. M. Bulheller, A. Rodger and J. D. Hirst, *Phys. Chem. Chem. Phys.*, 2007, **9**, 2020-2035.
51. J. Y. Su, R. S. Hodges and C. M. Kay, *Biochemistry*, 1994, **33**, 15501-15510.
52. V. Castelletto, I. W. Hamley, J. Seitsonen, J. Ruokolainen, G. Harris, K. Bellmann-Sickert and A. G. Beck-Sickinger, *Biomacromolecules*, 2018, **19,** 4230-4332.
53. L. Whitmore and B. A. Wallace, *Nucleic Acids Research*, 2004, **32**, W668-W673.
54. A. J. Miles and B. A. Wallace, *Chem. Soc. Rev.*, 2006, **35**, 39-51.
55. L. Whitmore and B. A. Wallace, *Biopolymers*, 2008, **89**, 392-400.
56. S. B. Jasim, Z. Li, E. E. Guest and J. D. Hirst, *J. Molec. Biol.*, 2018, **430**, 2196-2202.
57. J. Reed and A. Reed, *Anal. Biochem.*, 1997, **254**, 36-40.
58. I. W. Hamley , V. Castelletto, C. M. Moulton, J. Rodriguez-Perez, A. M. Squires, T. Eralp, G. Held, M. Hicks and A. Rodger, *J. Phys. Chem. B*, 2010, **114**, 8244-8254.
59. B. Stuart, *Biological Applications of Infrared Spectroscopy*, Wiley, Chichester, 1997.
60. A. Barth and C. Zscherp, *Quater. Rev. Biophys.*, 2002, **35**, 369-430.
61. W. K. Surewicz, H. H. Mantsch and D. Chapman, *Biochemistry*, 1993, **32**, 389-394.

62. M. Jackson and H. H. Mantsch, *Crit. Revi. Biochem. Molec. Biol.*, 1995, **30**, 95-120.
63. H. Hiramatsu and T. Kitagawa, *Biochim. Biophys. Acta*, 2005, **1753**, 100-107.
64. P. Haris and D. Chapman, *Biopolymers*, 1995, **37**, 251-263.
65. J. T. Pelton and L. R. McLean, *Anal. Biochem.*, 2000, **277**, 167-176.
66. H. Gaussier, H. Morency, M. C. Lavoie and M. Subirade, *Appl. Environ. Microbiol.*, 2002, **68**, 4803-4808.
67. F. Eker, K. Griebenow and R. Schweitzer-Stenner, *Biochemistry*, 2004, **43**, 6893-6898.
68. H. Fabian and W. Mantele, Handbook of Vibrational Spectroscopy, DOI: https://onlinelibrary.wiley.com/doi/pdf/10.1002/0470027320.s8201
69. A. Barth, *Prog. Biophys. Molec. Biol.*, 2000, **74**, 141-173.
70. A. Barth, *Biochim. Biophys. Acta-Bioenerg.*, 2007, **1767**, 1073-1101.
71. L. J. Bellamy, *The Infra-red Spectra of Complex Molecules*, Chapman and Hall, London 1975.
72. V. Castelletto, C. M. Moulton, G. Cheng, I. W. Hamley , M. R. Hicks, A. Rodger, D. E. López-Pérez, G. Revilla-López and C. Alemán, *Soft Matter*, 2011, **7**, 11405-11415.
73. Y. Liang, S. V. Pingali, A. S. Jogalekar, J. P. Snyder, P. Thiyagarajan and D. G. Lynn, *Biochemistry*, 2008, **47**, 10018-10026.
74. A. K. Mehta, K. Lu, W. S. Childers, S. Liang, J. Dong, J. P. Snyder, S. V. Pingali, P. Thiyagarajan and D. G. Lynn, *J. Am. Chem. Soc.*, 2008, **130**, 9829-9835.
75. J. Rodríguez-Pérez, I. W. Hamley , S. L. Gras and A. M. Squires, *Chem. Comm.*, 2012, **48**, 11835-11837.
76. D. A. Middleton, J. Madine, V. Castelletto and I. W. Hamley *Angew. Chem., Int. Ed. Engl.*, 2013, **52**, 10537-10540.
77. J. Rodriguez-Perez, I. W. Hamley and A. M. Squires, *Biomacromolecules*, 2011, **12**, 1810-1821.
78. L. A. Nafie, *Ann. Rev. Phys. Chem.*, 1997, **48**, 357-386.
79. T. A. Keiderling, *Curr. Opin. Chem. Biol.*, 2002, **6**, 682-688.
80. S. H. Shim, R. Gupta, Y. L. Ling, D. B. Strasfeld, D. P. Raleigh and M. T. Zanni, *Proc. Nat. Acad. Sci USA*, 2009, **106**, 6614-6619.
81. L. E. Buchanan, E. B. Dunkelberger, H. Q. Tran, P. N. Cheng, C. C. Chiu, P. Cao, D. P. Raleigh, J. J. de Pablo, J. S. Nowick and M. T. Zanni, *Proc. Nat. Acad. Sci USA*, 2013, **110**, 19285-19290.
82. Y. S. Kim, J. P. Wang and R. M. Hochstrasser, *J. Phys. Chem. B*, 2005, **109**, 7511-7521.
83. J. Ye, S. A. Fox, M. Cudic, E. M. Rezler, J. L. Lauer, G. B. Fields and A. C. Terentis, *J. Am. Chem. Soc.*, 2010, **132**, 980-988.
84. R. Nygaard, S. Nielbo, T. W. Schwartz and F. M. Poulsen, *Biochemistry*, 2006, **45**, 8350-8357.
85. J. F. Miravet, B. Escuder, M. D. Segarra-Maset, M. Tena-Solsona, I. W. Hamley, A. Dehsorkhi and V. Castelletto, *Soft Matter*, 2013, **9**, 3558-3564.
86. V. Castelletto, I. W. Hamley, M. D. Segarra-Maset, C. B. Gumbau, J. F. Miravet, B. Escuder, J. Seitsonen and J. Ruokolainen, *Biomacromolecules*, 2014, **15**, 591-598.
87. C. Felip-Leon, F. Galindo, J. F. Miravet, V. Castelletto and I. W. Hamley, *J. Phys. Chem. B*, 2017, **121**, 7443-7446.

88. P. R. Costa, D. A. Kocisko, B. Q. Sun, P. T. Lansbury and R. G. Griffin, *J. Am. Chem. Soc.*, 1997, **119**, 10487-10493.
89. T. L. S. Benzinger, D. M. Gregory, T. S. Burkoth, H. Miller-Auer, D. G. Lynn, R. E. Botto and S. C. Meredith, *Biochemistry*, 2000, **39**, 3491-3499.
90. A. B. Siemer, C. Ritter, M. Ernst, R. Riek and B. H. Meier, *Angew. Chem., Int.l Ed. Engl.*, 2005, **44**, 2441-2444.
91. H. Heise, W. Hoyer, S. Becker, O. C. Andronesi, D. Riedel and M. Baldus, *Proc. Nat. Acad. Sci USA*, 2005, **102**, 15871-15876.
92. J. J. Balbach, Y. Ishii, O. N. Antzutkin, R. D. Leapman, N. W. Rizzo, F. Dyda, J. Reed and R. Tycko, *Biochemistry*, 2000, **39**, 13748-13759.
93. B. Y. Ma and R. Nussinov, *Proc. Nat. Acad. Sci USA*, 2002, **99**, 14126-14131.
94. R. Tycko, *Curr. Opin. Struct. Biol.*, 2004, **14**, 96-103.
95. R. Tycko, *Quater. Rev. Biophys.*, 2006, **39**, 1-55.
96. T. Lührs, C. Ritter, M. Adrian, D. Riek-Loher, B. Bohrmann, H. Döbeli, D. Schubert and R. Riek, *Proc. Nat. Acad. Sci USA*, 2005, **102**, 17342-17347.
97. R. Nelson and D. Eisenberg, *Curr. Opin. Struct. Biol.*, 2006, **16**, 260-265.
98. R. Nelson and D. Eisenberg, *Adv. Protein Chem.*, 2006, **73**, 235-282.
99. R. Nelson and D. Eisenberg, *Curr. Opin. Struct. Biol.*, 2006, **16**, 260-265.
100. R. Nelson, M. R. Sawaya, M. Balbirnie, A. O. Madsen, C. Riekel, R. Grothe and D. Eisenberg, *Nature*, 2005, **435**, 773-778.
101. E. D. Eanes and G. G. Glenner, *J. Histochem. Cytochem.*, 1968, **16**, 673-677.
102. D. A. Kirschner, C. Abraham and D. J. Selkoe, *Proc. Nat. Acad. Sci USA*, 1986, **83**, 503-507.
103. M. Sunde and C. C. F. Blake, *Adv. Protein Chem.*, 1997, **50**, 123-159.
104. L. C. Serpell, *Biochim. Biophys. Acta*, 2000, **1502**, 16-30.
105. O. S. Makin and L. C. Serpell, *FEBS Journal*, 2005, **272**, 5950-5961.
106. I. W. Hamley, *Chem. Rev.*, 2017, **17**, 14015-14041.
107. K. Morris and L. Serpell, *Chem. Soc. Rev.*, 2010, **39**, 3445-3453.
108. O. S. Makin, P. Sikorski and L. C. Serpell, *J. Appl. Crystallogr.*, 2007, **40**, 966-972.
109. A. M. Squires, G. L. Devlin, S. L. Gras, A. K. Tickler, C. E. MacPhee and C. M. Dobson, *J. Am. Chem. Soc.*, 2006, **128**, 11738-11739.
110. D. Papapostolou, A. M. Smith, E. D. T. Atkins, S. J. Oliver, M. G. Ryadnov, L. C. Serpell and D. N. Woolfson, *Proc. Nat. Acad. Sci USA*, 2007, **104**, 10853-10858.
111. E. F. Banwell, E. S. Abelardo, D. J. Adams, M. A. Birchall, A. Corrigan, A. M. Donald, M. Kirkland, L. C. Serpell, M. F. Butler and D. N. Woolfson, *Nature Materials*, 2009, **8**, 596-600.
112. O. S. Makin and L. C. Serpell, *Fibre Diffraction Review*, 2004, **12**, 29-35.
113. M. M. Pallitto, J. Ghanta, P. Heinzelman, L. L. Kiessling and R. M. Murphy, *Biochemistry*, 1999, **38**, 3570-3578.
114. C.-L. Shen, M. C. Fitzgerald and R. M. Murphy, *Biophys. J.*, 1994, **67**, 1238-1246.
115. D. M. Walsh, A. Lomakin, G. B. Benedek, M. M. Condron and D. B. Teplow, *J. Biol. Chem.*, 1997, **272**, 22364-22372.
116. Y. Kusumoto, A. Lomakin, D. B. Teplow and G. B. Benedek, *Proc. Nat. Acad. Sci USA*, 1998, **95**, 12277-12282.
117. F. Sokolowski, A. J. Modler, R. Masuch, D. Zirwer, M. Baier, G. Lutsch, D. A. Moss, K. Gast and D. Naumann, *J. Biol. Chem.*, 2003, **278**, 40481-40492.

118. A. J. Modler, K. Gast, G. Lutsch and G. Damaschun, *J. Molec. Biol.*, 2003, **325**, 135-148.
119. B. J. Berne and R. Pecora, *Dynamic Light Scattering*, Wiley-Interscience, New York, 1976.
120. J. Stetefeld, S. McKenna and T. R. Patel, *Biophys. Rev.*, 2016, **8**, 409-427.
121. P. A. Hassan, S. Rana and G. Verma, *Langmuir*, 2015, **31**, 3-12.
122. I. W. Hamley *Introduction to Soft Matter. Revised Edition*, Wiley, Chichester, 2007.
123. I. W. Hamley, A. Dehsorkhi, P. Jauregi, J. Seitsonen, J. Ruokolainen, F. Coutte, G. Chataigné and P. Jacques, *Soft Matter*, 2013, **9**, 9572-9578.
124. A. Dehsorkhi, I. W. Hamley, J. Seitsonen and J. Ruokolainen, *Langmuir*, 2013, **29**, 6665-6672.
125. A. Dehsorkhi, R. J. Gouveia, A. M. Smith, I. W. Hamley, V. Castelletto, C. J. Connon, M. Reza and J. Ruokolainen, *Soft Matter*, 2015, **11**, 3115-3124.
126. J. S. Pedersen, *Adv. Colloid Interface Sci.*, 1997, **70**, 171-210.
127. I. W. Hamley , M. J. Krysmann, V. Castelletto, A. Kelarakis, L. Noirez, R. A. Hule and D. Pochan, *Chem. Eur. J.*, 2008, **14**, 11369-11374.
128. I. W. Hamley , M. J. Krysmann, V. Castelletto and L. Noirez, *Adv. Mater.*, 2008, **20**, 4394-4397.
129. G. Pabst, M. Rappolt, H. Amenitsch and P. Laggner, *Phys. Rev. E*, 2000, **62**, 4000-4009.
130. I. W. Hamley , A. Dehsorkhi and V. Castelletto, *Chem. Comm.*, 2013, **49**, 1850-1852.
131. www.sasfit.org
132. www.sasview.org/
133. F. Spinozzi, C. Ferrero, M. G. Ortore, A. D. Antolinos and P. Mariani, *J. Appl. Crystallogr.*, 2014, **47**, 1132-1139.
134. www.isis.stfc.ac.uk/Pages/Loq-software.aspx.
135. D. Svergun, C. Barberato and M. H. J. Koch, *J. Appl. Crystallogr.*, 1995, **28**, 768-773.
136. D. Franke, M. V. Petoukhov, P. V. Konarev, A. Panjkovich, A. Tuukkanen, H. D. T. Mertens, A. G. Kikhney, N. R. Hajizadeh, J. M. Franklin, C. M. Jeffries and D. I. Svergun, *J. Appl. Crystallogr.*, 2017, **50**, 1212-1225.
137. D. Schneidman-Duhovny, M. Hammel, J. A. Tainer and A. Sali, *Biophys. J.*, 2013, **105**, 962-974.
138. D. Schneidman-Duhovny, M. Hammel, J. A. Tainer and A. Sali, *Nucleic Acids Res.*, 2016, **44**, W424-W429.
139. D. K. Putnam, E. W. Lowe and J. Meiler, *Comput. Struct. Biotech. J.*, 2013, **8**, e201308006.
140. K. Lu, J. Jacob, P. Thiyagarajan, V. P. Conticello and D. G. Lynn, *J. Am. Chem. Soc.*, 2003, **125**, 6391-6393.
141. I. W. Hamley, S. Burholt, J. Hutchinson, V. Castelletto, E. R. da Silva, W. A. Alves, P. Gutfreund, L. Porcar, R. Dattani, D. Hermida-Merino, G. E. Newby, M. Reza, J. Ruokolainen and J. Stasiak, *Biomacromolecules*, 2017, **18**, 141-149.
142. I. W. Hamley, A. Dehsorkhi, V. Castelletto, S. Furzeland, D. Atkins, J. Seitsonen and J. Ruokolainen, *Soft Matter*, 2013, **9**, 9290-9293.
143. J. Adamcik and R. Mezzenga, *Curr. Opin. Colloid Interface Sci.*, 2012, **17**, 369-376.
144. I. Usov, J. Adamcik and R. Mezzenga, *Faraday Discuss.*, 2013, **166**, 151-162.

145. I. Usov and R. Mezzenga, *ACS Nano*, 2014, **8**, 11035-11041.
146. I. Usov and R. Mezzenga, *Macromolecules*, 2015, **48**, 1269-1280.
147. J. Adamcik, C. Lara, I. Usov, J. S. Jeong, F. S. Ruggeri, G. Dietler, H. A. Lashuel, I. W. Hamley and R. Mezzenga, *Nanoscale*, 2012, **4**, 4426-4429.
148. J. Adamcik, V. Castelletto, I. W. Hamley and R. Mezzenga, *Angew. Chem., Int. Ed. Engl.*, 2011, **50**, 5495-5498.
149. H. Cui, T. K. Hodgdon, E. W. Kaler, L. Abezgaous, D. Danino, M. Lubovsky, Y. Talmon and D. J. Pochan, *Soft Matter*, 2007, **3**, 945-955.
150. H. Friedrich, P. M. Frederik, G. de With and N. Sommerdijk, *Angewandte Chemie-International Edition*, 2010, **49**, 7850-7858.
151. D. Danino, *Curr. Opin. Colloid Interface Sci.*, 2012, **17**, 316-329.
152. J. Lebowitz, M. S. Lewis and P. Schuck, *Protein Science*, 2002, **11**, 2067-2079.
153. P. Schuck, *Analytical Biochemistry*, 2003, **320**, 104-124.
154. G. W. M. Vandermeulen, C. Tziatzios and H.-A. Klok, *Macromolecules*, 2003, **36**, 4107-4114.
155. C. J. Pike, D. Burdick, A. J. Walencewicz, C. G. Glabe and C. W. Cotman, *J. Neuroscience*, 1993, **13**, 1676-1687.
156. T. Bartels, J. G. Choi and D. J. Selkoe, *Nature*, 2011, **477**, 107-U123.
157. A. M. Smith, T. R. Jahn, A. E. Ashcroft and S. E. Radford, *J. Molec. Biol.*, 2006, **364**, 9-19.
158. P. Schuck, *Biophysical Journal*, 2000, **78**, 1606-1619.
159. L. M. D. Rodriguez, Y. Hemar, J. Cornish and M. A. Brimble, *Chem. Soc. Rev.*, 2016, **45**, 4797-4824.
160. B. Escuder, F. Rodriguez-Llansola and J. F. Miravet, *New J. Chem.*, 2010, **34**, 1044-1054.
161. C. Tomasini and N. Castellucci, *Chem. Soc. Rev.*, 2013, **42**, 156-172.
162. C. W. Macosko, *Rheology. Principles, Measurements and Applications*, VCH, New York, 1994.
163. L. L. E. Mears, E. R. Draper, A. M. Castilla, H. Su, Zhuola, B. Dietrich, M. C. Nolan, G. N. Smith, J. Doutch, S. Rogers, R. Akhtar, H. G. Cui and D. J. Adams, *Biomacromolecules*, 2017, **18**, 3531-3540.
164. V. Castelletto, R. H. Barnes, K. A. Karatzas, C. J. C. Edwards-Gayle, F. Greco, I. W. Hamley, R. Rambo, J. Seitsonen and J. Ruokolainen, *Biomacromolecules*, 2018, **19**, 2782-7294.

Figures

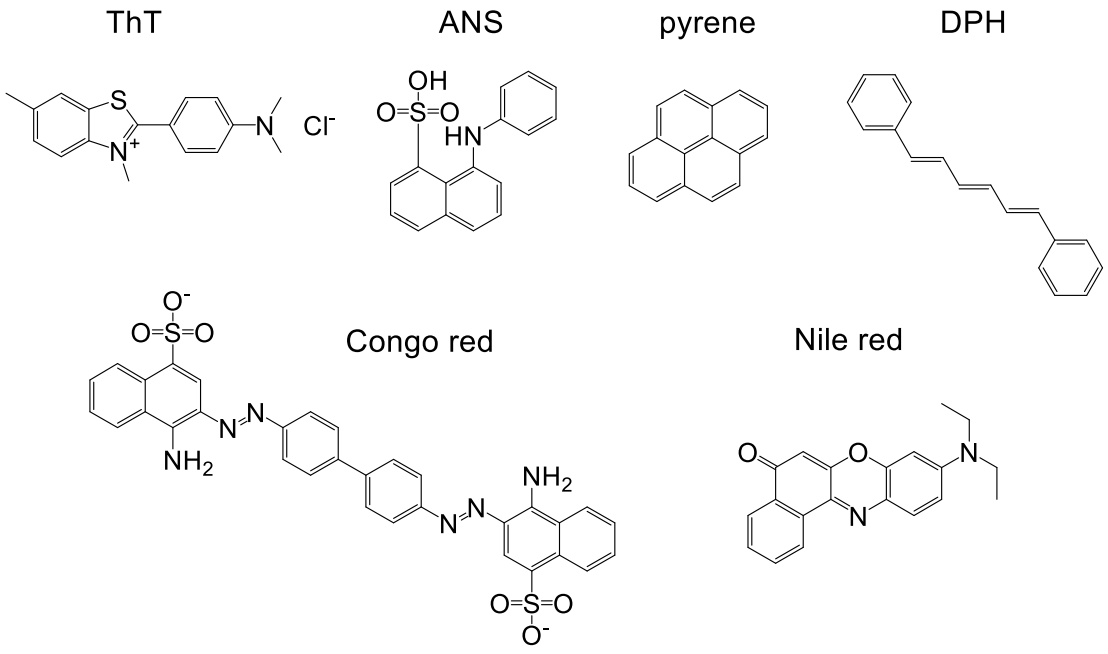

Fig.1. Molecular structure of fluorescent probe dyes mentioned in the text, used to stain peptide structures or in assays of aggregation.

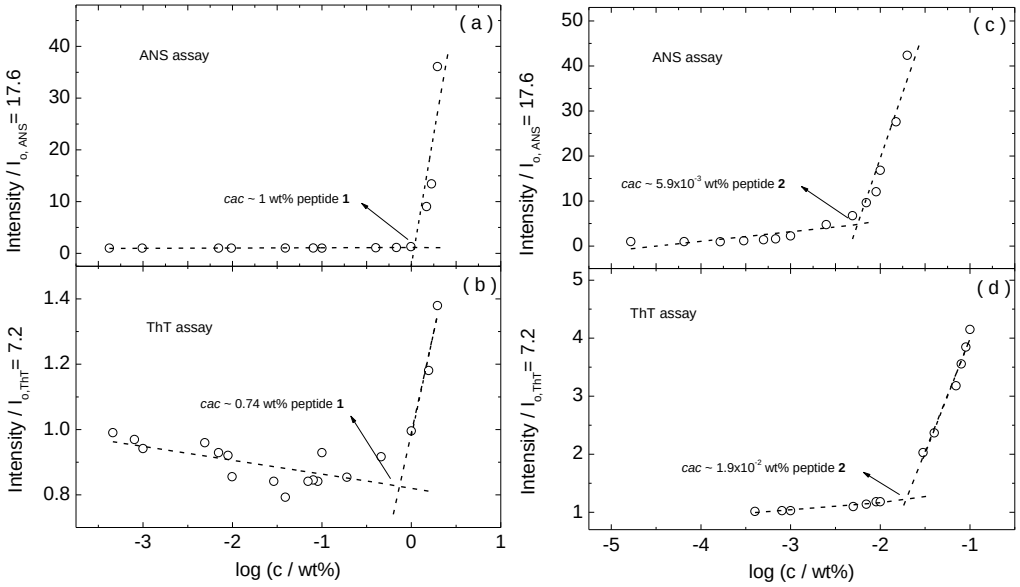

Fig.2. Comparison of critical aggregation concentration (*cac*) assays for amyloid forming peptides using different fluorescent probes: (a) ANS fluorescence for NH_2-KLVFF-$CONH_2$, (b) ThT fluorescence for NH_2-KLVFF-$CONH_2$, (c) ANS fluorescence for NH_2-KLVFF-$CONH_2$, (d) ThT fluorescence for NH_2-K(Boc)LVFF-$CONH_2$.[23]

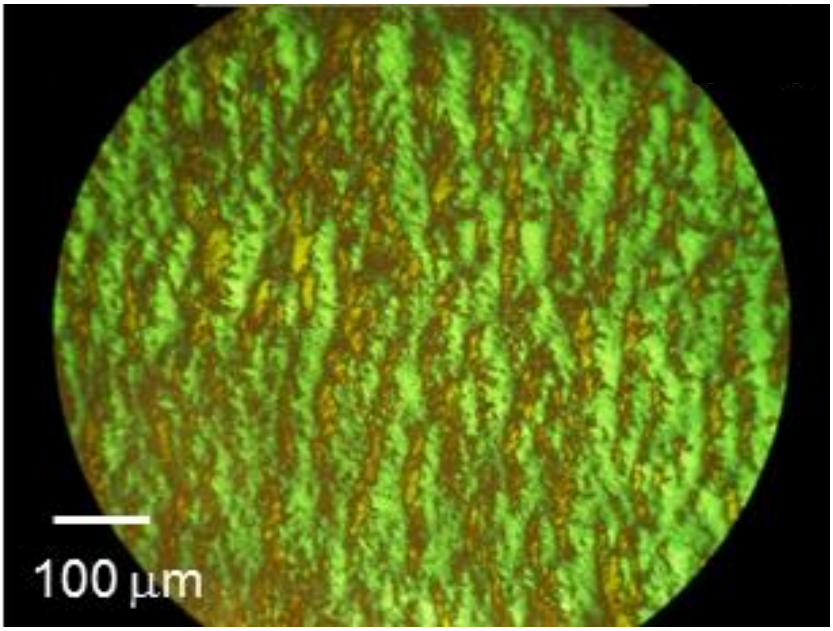

Fig.3. Congo red staining of β-sheet "amyloid" fibrils formed by lipopeptide C_{16}-YEALRVANEVTLN.[40]

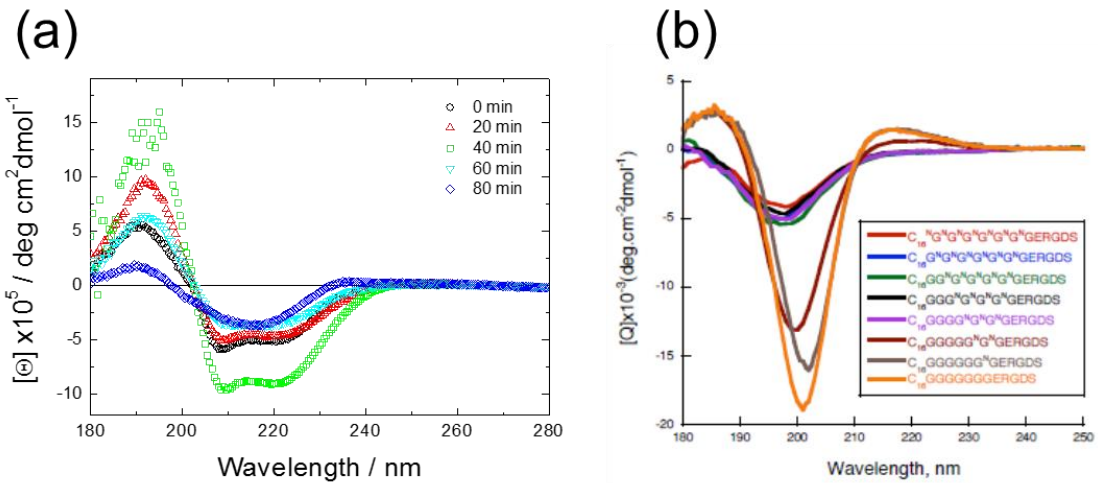

Fig.4. Representative peptide CD spectra from different secondary structures. (a) CD spectra showing transition from α-helix (black squares) to β-sheet (blue diamonds) during annealing of peptide PYY11 at pH 8.47 and 2 wt% at 56 °C. Adapted from ref.[17] (b) Contrasting CD spectra for PPII (magenta, grey and orange family of curves) and disordered conformations (other curves) from 2 wt% solutions of the indicated lipopeptides.[47]

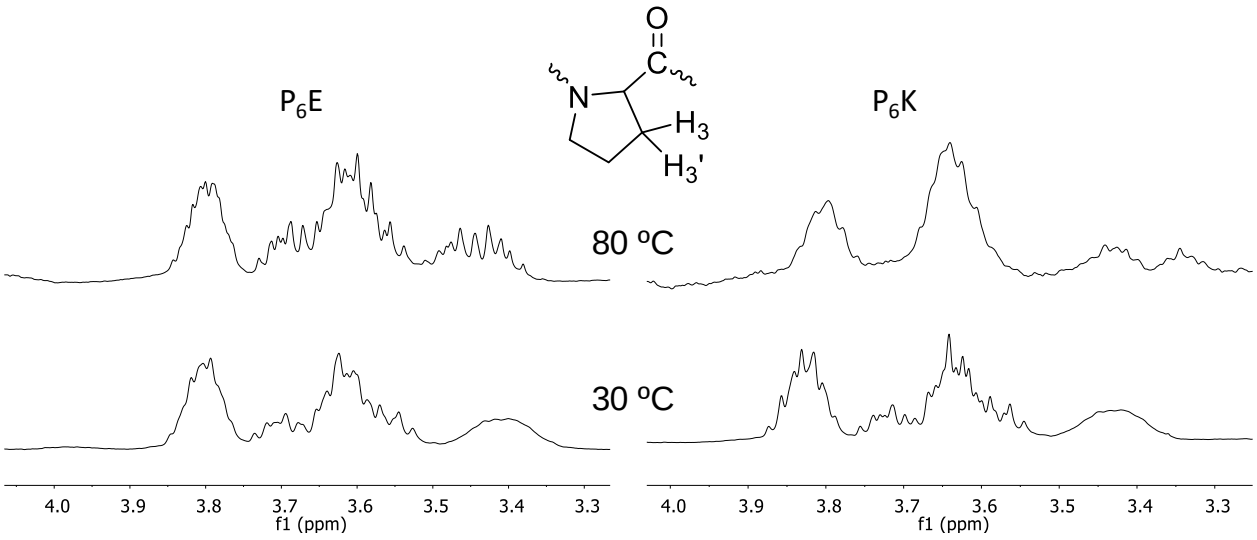

Fig.5. Partial ^{1}H NMR spectra of surfactant-like peptides P_6E and P_6K (0.1% w/w, pH 7) at 25 ºC and 80 ºC.[87]

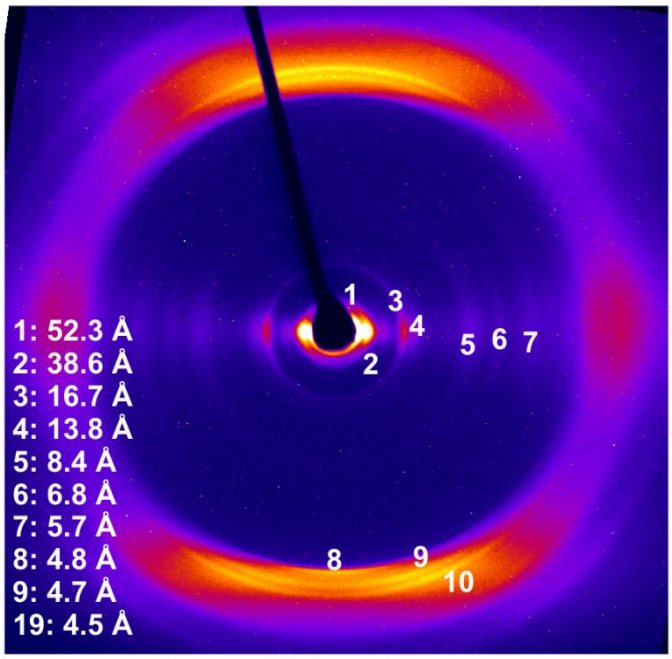

Fig.6. Fibre XRD pattern obtained from a dried stalk of lipopeptide C_{16}-GGGRGDS with reflections indexed as indicated.[11]

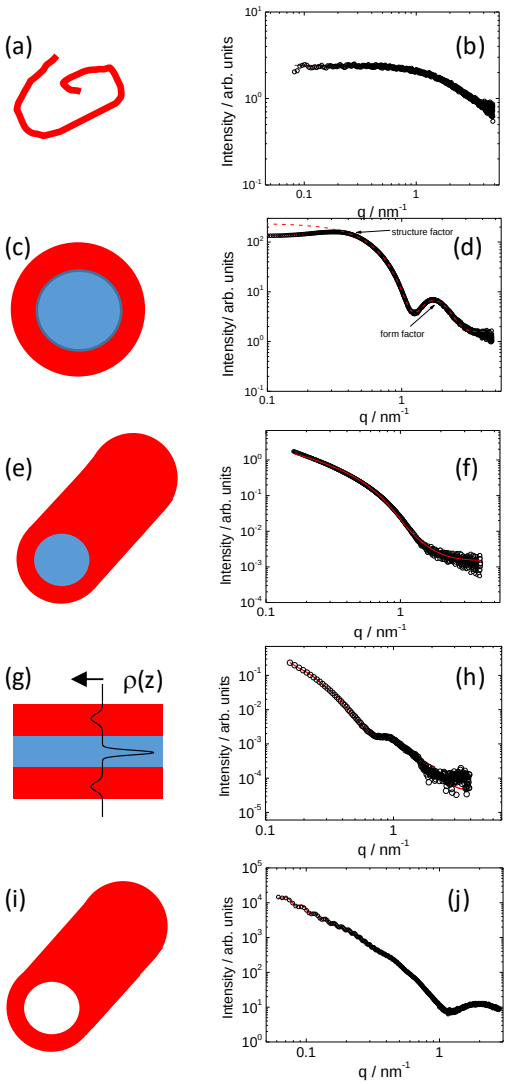

Fig.7. Examples of fitted SAXS data: (a) Gaussian coil representing a monomeric peptide, (b) SAXS data for a 1 wt% aqueous solution of P_6E (open symbols) with fit to Gaussian coil form factor (red line),[24] (c) Sketch of core-shell spherical micelle, (d) SAXS data from a 1 wt% solution of lipopeptide $C_{16}CSK_4RGDS$ with fit to core-shell micelle form factor (dashed red line, fit parameters in Table S1) and also allowing for structure factor (solid red line) (e) Schematic of core-shell cylinder, (f) SAXS data for a 1 wt% aqueous solution of A_6R (open symbols) with fit to core-shell cylinder form factor (red line),[164] (g) Schematic of a bilayer with superposed electron density profile represented by bilayer Gaussian model (three Gaussian representation), with large dip in the lipid interior (blue lamella) and positive relative electron density in the peptide headgroup regions (red domains), (h) SAXS data for an 0.5 wt% aqueous solution of lipopeptide C_{16}-YEALRVANEVTLN (open symbols) with Gaussian bilayer form factor fit,[40] (i) Schematic of a nanotube, (j) SAXS data for an 1 wt% aqueous solution of lipopeptide C_{16}-KKFFVLK (open symbols) with nanotube (i.e. hollow cylindrical shell) + Gaussian bilayer (to account for electron density cross-section across the nanotube wall) form factor fit.[142]

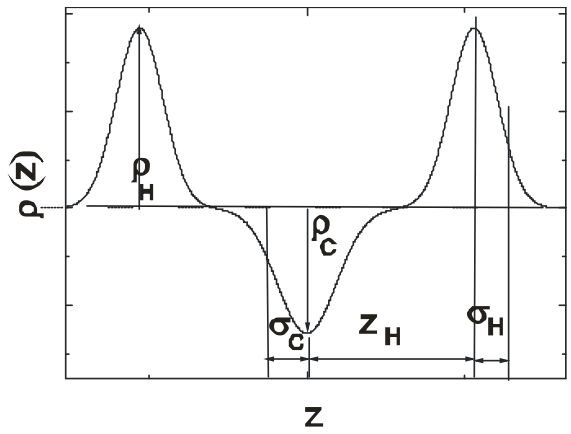

Fig.8. Detailed parameterization of electron density profile across a bilayer (e.g. lipopeptide bilayer), parameterized using three Gaussian functions. Here ρ_H and ρ_C denote the electron density of the headgroup and hydrophobic core respectively and σ_H and σ_C are the widths of the corresponding Gaussian functions, Z_H is the offset distance of the Gaussians representing the headgroup densities.[11]

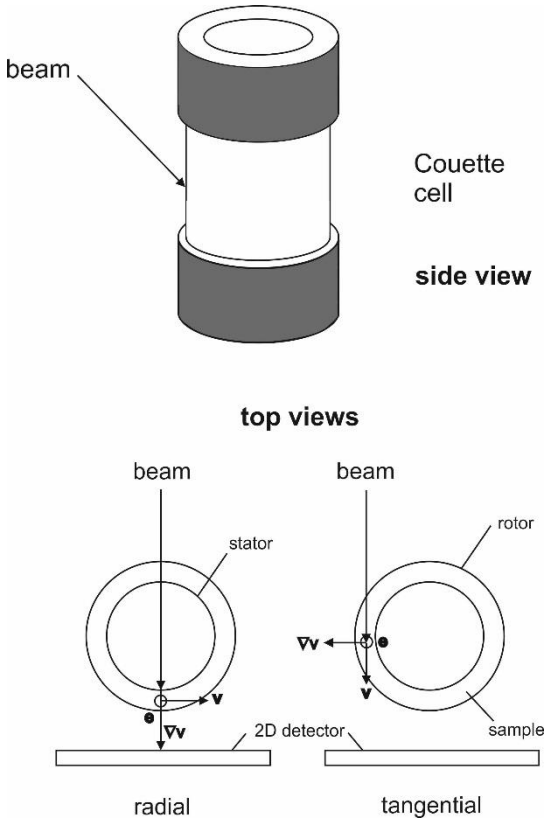

Fig.9. Definitions of Couette geometry and shear axes.[141]

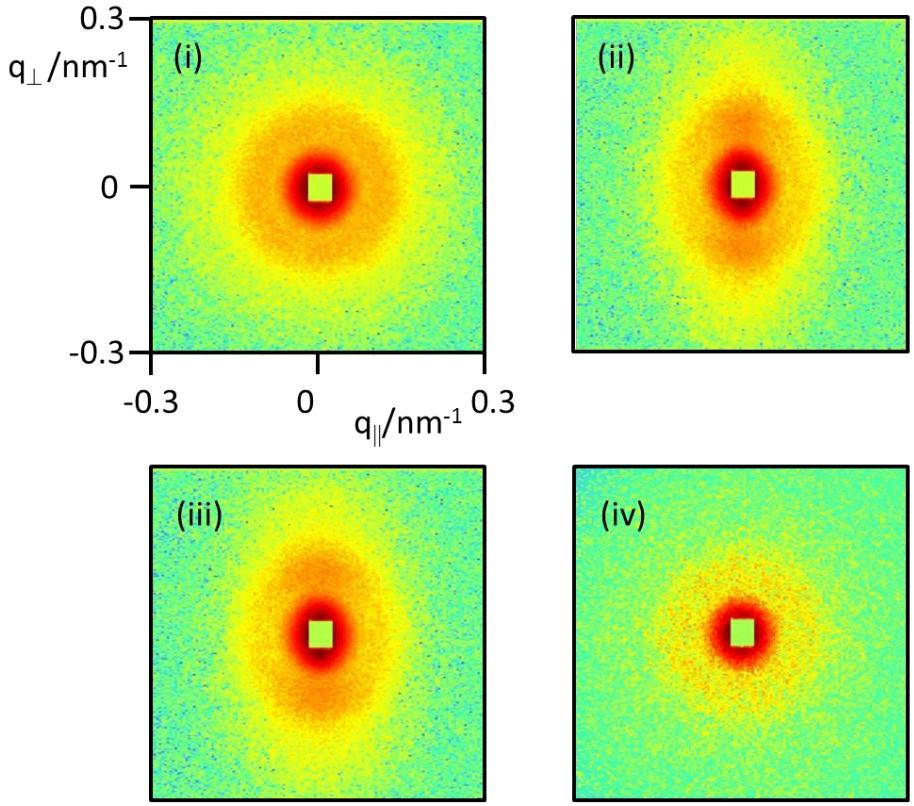

Fig.10. SANS patterns obtained from a 1 wt% solution of RFL_4FR in D_2O in the radial configuration.[141] (i) Zero shear (ii) under shear at $\dot{\gamma}$ = 100 s^{-1}, (iii) under shear at $\dot{\gamma}$ = 1000 s^{-1}, (iv) Following shear at $\dot{\gamma}$ = 1000 s^{-1}. The shear direction is horizontal and the intensity scale is logarithmic.

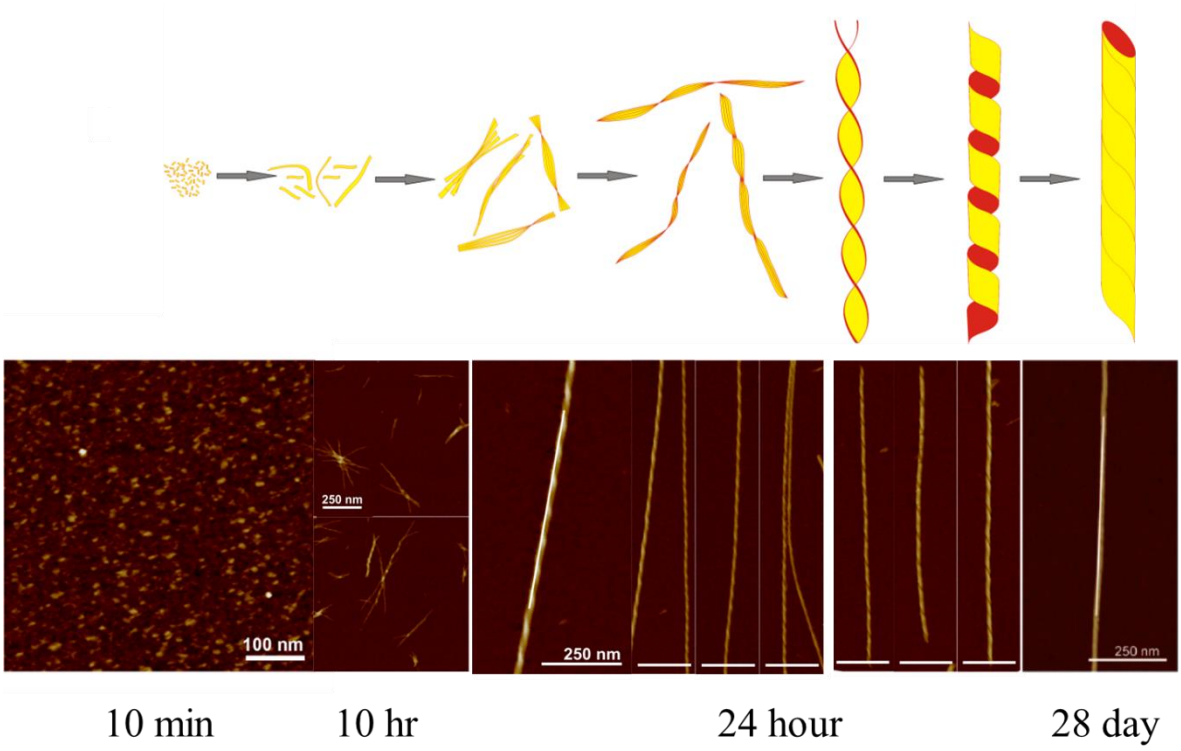

Fig.11. Bottom: AFM height images during the time-dependent aggregation of peptide CH_3CONH-βAβAKLVFF-$CONH_2$ during incubation at 25 ^oC. After 10 min small oligomers are observed, after 10 hr nucleation of protofilaments is evident, but after 24 hr twisted tapes and helical ribbons are formed. Finally, after 28 days of incubation at 4 ^oC. Top: schematic of the corresponding structures. Adapted from ref.[148]

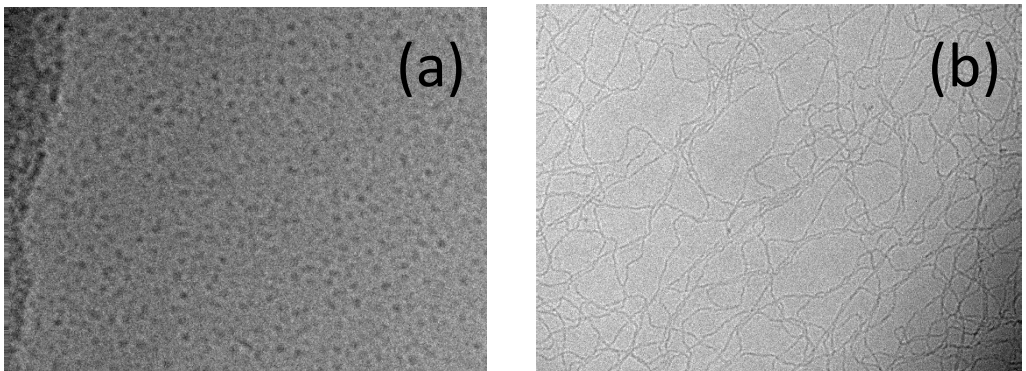

Fig.12. Representative cryo-TEM images from different classes of peptide nanostructures. (a) Spherical micelles in a 0.5 wt% solution of C_{16}-CSK_4RGDS, (b), fibrils formed in a 0.5 wt% solution of lipopeptide PYY17 at pH 8. (c) Twisted tapes formed in a 2 wt% solution of peptide GNNDESNISFKEK, (d) Nanotubes formed in a 1 wt% solution of C_{16}-KKFFVLK.

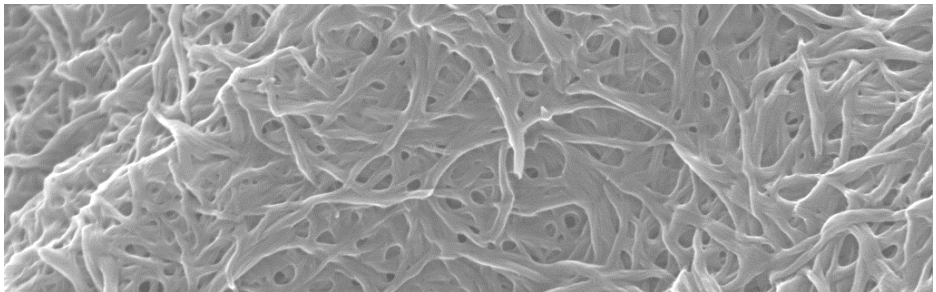

Fig.13. SEM image of a fibril hydrogel of lipopeptide C_{14}-YEALRVANEVTLN (prepared from 1 wt% sample).[40]

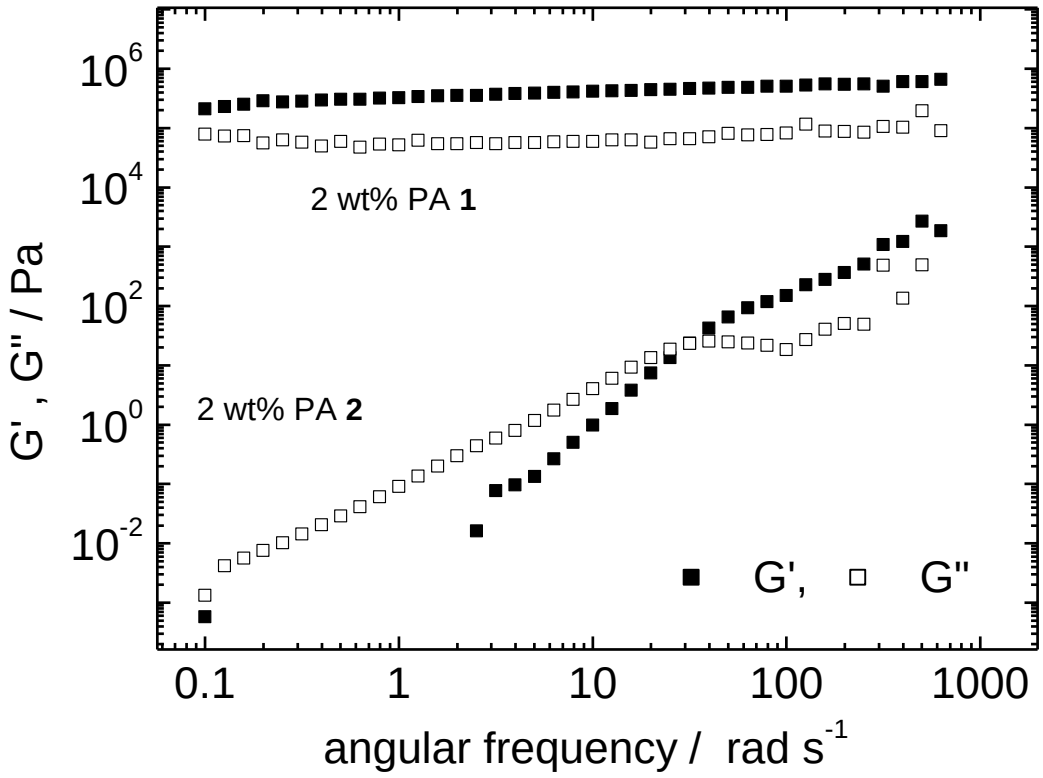

Fig. 14. Dynamic shear moduli measured for 2 wt% samples of peptide amphiphiles PA **1** C_{16}-GGGRGD and PA **2** C_{16}-GGGRGDS.[11]

Table 1. SAXS Fit Parameters for Fig.7d.

Parameter / **Sample**	R / nm	ΔR/ nm	R_2/ nm	μ	η	BG	R_{HS}	f_p
C_{16}CSK4RGDS 1%	**2.32**	**0.76**	**1.36**	**- 0.745**	**0.193**	**1.45**	**5.90**	**0.074**

Key. *FORM FACTOR PARAMETERS*: *R*: outer radius, Δ*R*: polydispersity (Gaussian half width) in *R*, R_2: inner radius, μ: relative scattering contrast (electron density) of core, η: scattering constrast of shell, BG: background. *STRUCTURE FACTOR PARAMETERS*: R_{HS}: hard sphere radius, f_p = volume fraction of hard spheres.